Development of Nanobainitic Microstructures in Carbo-Austempered Cast Steels: Heat Treatment, Microstructure and Properties

Oscar Ríos-Diez [1] , **Ricardo Aristizábal-Sierra** [1,*], **Claudia Serna-Giraldo** [1] , **Jose A. Jimenez** [2] **and Carlos Garcia-Mateo** [2,*]

[1] Gipimme, Department of Materials Engineering, Engineering Faculty, Universidad de Antioquia, Calle 67 No. 53-108, Bloque 18, Oficina 240, Medellín 050010, Colombia; eduardo.rios@udea.edu.co (O.R.-D.); claudia.serna@udea.edu.co (C.S.-G.)

[2] MATERALIA Research Group, Department of Physical Metallurgy, National Center for Metallurgical Research (CENIM-CSIC), Avenida Gregorio del Amo, 8, 28040 Madrid, Spain; jimenez@cenim.csic.es

* Correspondence: ricardo.aristizabal@udea.edu.co (R.A.-S.); cgm@cenim.csic.es (C.G.-M.); Tel.: +57-4-219-8546 (R.A.-S.); +34-91-553-8900 (C.G.-M.)

Abstract: Carburizing implies the existence of a carbon gradient from the surface to the core of the steel, which in turn will affect both the critical temperature for austenite formation and the kinetics of the bainitic transformation during the austempering treatment. Therefore, for future development of carbo-austempered steels with nanobainitic microstructures in the case, it is key to understand the effect of such carbon gradient has on the final microstructure and the mechanical properties reached by the heat treatments used. This work was divided into two parts, firstly two alloys with similar carbon content to those at the surface and center of the carburized steel were used to establish the optimal heat treatment parameters and to study bainite transformation kinetics by high resolution dilatometry. In a second step, a carburized alloy is produced and subjected to the designed heat treatments, in order to evaluate the microstructure and mechanical properties developed. Results thus obtained are compared with those obtained in the same carburized alloy after following the most common quench and temper treatment.

Keywords: carbo-austempering; intercritical austenitization; isothermal transformation; multiphasic structures; bainitic transformation

1. Introduction

In recent decades, nanobainitic steels have been the subject of countless research papers and reviews, especially on topics related to the mechanism of transformation, mechanical performance, optimization of the processing routes and tempering resistance of the microstructure. According to Bhadeshia et al. [1,2], bainite transformation is best described as a diffusionless and displacive reaction in which nucleation happens by a paraequilibrium mechanism, where only C diffuses, and growth occurs with no change in the chemical composition of the parent and product phases. Because of the displacive nature of the bainitic reaction, Garcia-Mateo et al. [3] explained that the size of the microstructure is governed by the mechanical strength of the parent austenite, thus a stronger parent austenite will produce a finer microstructure that in turn will exhibit better mechanical properties.

According to Morales-Rivas et al. [4], nanobainitic steels exhibit the highest strength/toughness combinations (2 GPa/30 MPa m$^{1/2}$) among bainitic steels. The microstructure consist mainly of two phases: bainitic ferrite (α_b) and carbon-enriched retained austenite (γ_{ret}) that is obtained after a simple isothermal heat treatment at a temperature between the bainite and martensite start

transformations, Bs and Ms, respectively. The typical chemical composition range for nanobainitic steel is (0.6–1.0)C-(1.5–2.0)Si-(0.7–2.0)Mn-(0.4–1.7)Cr wt.%, which ensures both the necessary hardenability to avoid any undesirable transformation to ferrite or pearlite, and the occurrence of the bainitic reaction at low transformation temperatures.

Among the most novel proposals in the applicability and processing of nanobainitic steels, the heat treatment of carbo-austempering stands out. Hayrynen et al. [5] explained that conventional carbo-austempering methods for surface steels involve quenching immediately following carburizing at 850–950 °C at a temperature above the case Ms, or cooling to room temperature and later reheating the surface-carburized steel to 850–950 °C and then quenching at a temperature above case Ms. When this process is applied to a carburized low carbon steel (<0.3 wt.%), a bainitic case and low carbon martensitic core are produced.

Although quench and temper (Q&T) are well stablished approaches to obtain complex microstructures than can lead to a combination of strength, ductility and toughness in high silicon steels, there are several reasons to use austempering in production instead.

According to Damon et al. [6], the amount of shape distortion is generally lower after austempering treatments because the bainitic transformation occurs at a single temperature with lower expansion and internal stresses. Thus, cracking during the heat treatment can be avoided, the final grinding time shortened and cost of the final work piece reduced.

The tempering process allows the relaxation of residual stresses formed during the initial quenching process, and then compressive surface residual stresses will be higher and extended to a deeper depth in austempered samples than in Q&T materials, resulting in better fatigue performance and higher wear resistance than conventional carburizing Q&T [5,7].

Finally, another reason to use austempering instead of Q&T is that the amount of austenite retained at room temperature after quenching is lower than the retained austenite (γ_{ret}) fraction in austempering treatment. As austenite is able to accommodate a higher amount of plastic deformation than bainitic ferrite and martensite by dislocation slip or secondary deformation mechanisms such as martensitic transformation (TRIP effect), a higher amount of austenite will increase the ductility and toughness of the final product.

Carbo-austempered process has been successfully applied for the manufacture of typical Q&T components as bearings that are used in reduced impact and lubrication conditions, required for railway applications, rolling mills, cranes and drills [8], as well as for automotive components as gears, pinions and high stressed components where high wear and fatigue resistance are important [5].

On the other hand, steels with high tensile strength, high ductility and a high strain hardening coefficient, known as TRIP steels, could be derived from a structure consisting of ferrite (α), bainitic ferrite (α_b), martensite (α') and retained austenite (γ_{ret}). The high ductility is due to the presence of a ferritic matrix (α) and the ability of the γ_{ret} to transform into martensite (α') when subjected to an external stress/strain, which in turn increases the strain-hardening coefficient. Morales-Rivas et al. [9] reported that the high mechanical strength is derived from the presence of α_b and α' within the microstructure. This type of microstructure can be achieved by intercritical austenitizing followed by isothermal transformation in the bainitic temperature range of alloys with the right concentration of carbon, silicon, manganese and chromium.

Carburizing implies the existence of a carbon gradient, thus there are differences in the temperature required for the whole austenitization of the microstructure and the amount of bainitic ferrite through the thickness of the carburized steel. A better understanding of these differences will allow tailoring the heat treatment parameters to produce carbo-austempered steels with nanobainitic microstructures at the case. This work aimed to a better understanding of the effect of carbon concentration and heat treatment parameters on the microstructure and mechanical properties of carbo-austempered steels with nanobainitic microstructures in the case. The evaluation included an austenitizing condition that produced full austenitizing in the case and partial austenitizing in the core of the carburized steel,

since it is hypothesized that, in carbo-austempering steels, the combination of properties obtained from a gradually changing microstructure (from the surface to the core) would be ideal.

2. Materials and Methods

Two alloys with similar carbon content to those to be reached at the surface and center of the carburized Steel (0.29 wt.% and 0.76 wt.%, respectively) were prepared in a 50-kW induction furnace (Inductotherm, Sanand, India) at the casting laboratory of the Universidad de Antioquia, Medellin-Colombia. For this purpose, low carbon steel, graphite, ferrosilicon, ferrochromium and ferromanganese were used as charging materials. After melting, the steels were deoxidized with 0.1% of aluminum and poured at around 1620 °C into sodium silicate-CO_2 bonded sand molds to obtain 25-mm thick Y-blocks. Chemical composition of the as-cast alloys determined by optical emission spectrometry (OES) in a Bruker Q8 Magellan (Bruker, Karlsruhe, Germany) are given in Table 1. Notice that silicon, manganese and chromium in both steels are at the same level, thus the main difference between the steels is the carbon concentration.

Table 1. Chemical composition of the steels, all in wt.%.

C	Si	Mn	Cr	Observations
0.29	1.87	0.55	0.92	core steel
0.76	1.82	0.53	0.93	case steel

In order to minimize the chemical segregation of the solidification process and eliminate the as-cast microstructure, the steels were homogenized at 1150 °C for 48 h in vacuum and then slowly cooled at a rate of 4 °C/s. The microstructure thus produced consisted of polygonal α (55%) and pearlite colonies (45%) with an ASTM 6.5-grain number in the core steel, while in the case steel the microstructure was fully pearlitic with an ASTM 7-grain number. Note that grain size of the homogenized microstructures were determined according to the standard ASTM International [10].

Some of the thermal treatments, as well as the determination of critical transformation temperatures, Ac1, Ac3, and Ms, and the kinetics of the bainitic transformation were determined using 4-mm diameter and 10-mm length cylinders in a BAHR 805A (TA Instruments, Hüllhorst, Germany) high-resolution dilatometer. The heating system consists of an induction coil and cooling is applied by blowing helium to the sample, while temperature is controlled by a type-K thermocouple welded to the central part of the sample surface. The dilatometry test was performed using a specific module, equipped with fused silica push-rods to measure the longitudinal changes during different stages of the heat treatments.

The specimens were sectioned and polished following a conventional metallographic technique and the microstructure was revealed by etching with Nital 2% (2 mL of HNO_3 + 98 mL of Ethanol) and Picral 4% (4 g picric acid + 100 mL of ethanol), the latter only in the intercritical treatments. The microstructure was analyzed by light optical microscopy (LOM) (Nikon MA100 Niko Instrument Inc, Melville, NY, USA) and scanning electron microscopy (SEM) (JEOL-JSM 6490LV JEOL Ltd, Tokyo, Japan). The volume fraction of ferrite (α) and martensite (α'), obtained in the core steel after intercritical austenitization and quenching, was measured by systematic point counting according to the ASTM International [11]. α_b plates and γ_{ret} thin film thicknesses were measured according to the methodology described by Garcia-Mateo et al. [12]. It is based on the measurement of linear intercepts on SEM micrographs plus a subsequent stereological correction applied to the mean linear intercept.

On the other hand, X-ray diffraction (XRD) was used to measure the fraction and C content of retained austenite, Vγ and Cγ, respectively. For this purpose, a Panalytical Empyrean 2012 (PANanalytical B.V., Almelo, The Netherland) diffractometer with Co Kα, working at 40 kV and 100 mA was used. XRD data were collected over the 2θ range of 30° to 110° at a rate of 0.06 °min^{-1}. In this study, version 4.2 of Rietveld analysis program DIFFRACplus TOPAS (Bruker AXS GmbH, Karlsruhe, Germany, 2009) was used for the quantitative analysis of the crystalline phases present from the XRD patterns. Besides, this refinement included explicitly other parameters like lattice parameters.

The structural model used in the refinement was a combination of ferrite and austenite. Austenite carbon content was estimated using the well-known Dyson and Holmes' equation that relates the austenite lattice parameter to its composition [13]. Following standard metallographic procedures, XRD sample preparation includes a final set of cycles of etching and polishing in order to remove the plastically deformed surface layer that had been introduced during the grinding step.

Tensile and impact toughness (V-notch) specimens of the low carbon alloy (0.29 wt.% C) were cut and machined by a computer numerical control machine, according to the standard ASTM International [14,15], respectively. Later, the machined specimens, and a coupon sample, were carburized in a controllable gas-carburizing furnace. An endothermic gas enriched with propane gas was used as carburizer and the carburization temperature and time were 920 °C and 4 h, respectively. The carbon potential (Cp) value was 1% during the first hour, and it was changed to 0.8% during the last 3 h. Then, the specimens were cooled inside the furnace to room temperature.

In order to guaranty the homogeneity of the carburized layer, the coupon samples and a set of Charpy and tensile specimens were sacrificed to measure the carbon content distribution from the top surface to the core. For this purpose, OES previously calibrated using three standard samples of known C content, i.e., 0.18 wt.%, 0.57 wt.% and 0.9 wt.%, was used. The C profile was obtained by polishing the specimens to specific depths in steps of 100 μm where C content was measured, and a final 20-point C distribution with depth from the carburized surface was obtained.

The specimens were then thermally treated in order to develop the desired microstructures following the parameters given later in this paper. Austenitization was performed in an electric furnace in a vacuum atmosphere, followed by immersion in isothermal baths (a mixture of 40–50% sodium nitrate and 50–60% potassium nitrate salts with a melting point of 180 °C). For comparison purposes, a set of carburized samples were subjected to the standard industrial Q&T process for this type of steel; in accordance with the provisions by Parrish [16], quenching from 900 °C to room temperature was done in oil, followed by tempering at 250 °C for 120 min.

Tension test was carried out at room temperature using an INSTRON 5984 machine with 150-kN (Instron, Darmstadt, Germany) loading capacity at $3\,\text{s}^{-1}$ in round sub-size tensile specimens with a gauge diameter of 6 mm. An extensometer set to a gauge length of 20 mm was used for strain measurement. At least three specimens were tested for each condition and the average and standard deviation were calculated. The impact toughness was evaluated in V-notch 10 mm × 10 mm × 55 mm specimens by using a Karl Frank GMBH-300 J Charpy testing machine (Karl Frank GmbH, Weinheim-Birkenau, Germany) at room temperature. Three specimens were tested for each condition. Hardness Vickers HV10 measurements were made using an Harterprufer-Swiss Max 300 hardness testing machine (Gnehm Härteprüfer AG, Thalwil, Switzerland); at least five indents were made on each sample and the average values were taken. Finally, the microhardness profile of the heat-treated carburized surfaces was obtained using a Vickers tester Shimadzu HMV-G 20DT (Shimazu, Kyoto, Japan) under an applied load of 300 g for 10 s.

3. Results

3.1. Determination of the Austenitization Conditions

In order to determine the critical transformation temperatures, dilatometric samples of the core and case steels were heated at 0.18 °C/s up to 1000 °C, held for 10 min and finally quenched at 100 °C/s. The results of the dilatometric test showed the expected contraction of the $\alpha + \gamma$ field, as C increases. From the relative change in length (RCL) vs. temperature curves, Figure 1, on heating and cooling segments, Ac1, Ac3 temperatures were calculated following the procedures described by Garcia-De Andres et al. [17] and Ms temperatures were determined according to the Sourmail et al. protocol [18]. Note that selection of the heating conditions is adapted to those industrially doable, with the provisions by Parrish [16], as a function of the initial microstructure and critical thickness of the samples. Table 2 gathers the exact values of such temperatures. For the purpose of this work, the foreseen austenitisation

T is such that, while the case is fully austenitic, the core is still in the $\alpha + \gamma$ field; the results in Table 2 offered a processing window between 825–857 °C.
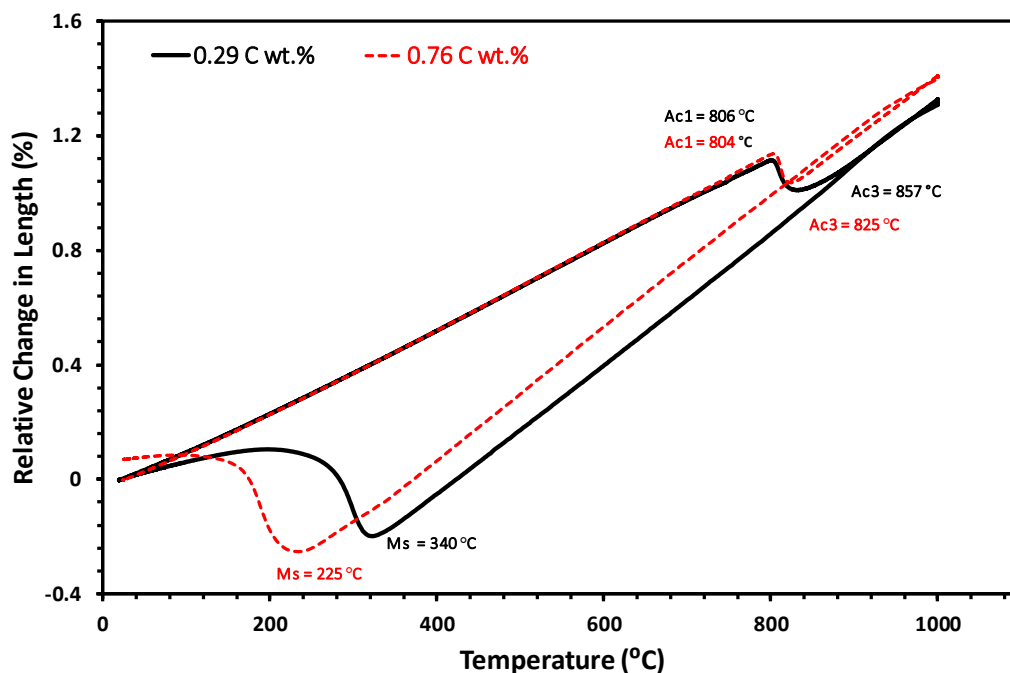

Figure 1. Relative change in length (RCL) as a function of T during 0.18 °C/s heating up to 1000 °C and subsequent cooling down to room temperature, 100 °C/s, for both alloys.

Table 2. Critical temperatures of the tested alloys, obtained by high-resolution dilatometry.

C (wt.%)	T (°C)		
	Ac1	Ac3	Ms
0.29	806	857	340
0.76	804	825	225

With that T range in mind, samples of both steels were heated from room temperature to the austenitization conditions given in Table 3 followed by quenching at 35 °C/s. Considering the critical temperatures shown in Table 2, some α remains untransformed in the core alloy during holding at 850, 840 and 830 °C, causing an enrichment of C on the remaining γ and, therefore, a change in the beginning temperature of the martensitic and bainitic transformations. The 0.76-wt.% C alloy remained in the single austenitic region for all the evaluated conditions. In terms of austenitization, the effect of the original microstructure is manifested as a change in the critical temperatures of phase transformations and in the growth rate of austenite as the holding temperature or time increases. For this reason, two different austenitization times were considered, $t_\gamma = 15$ min and 30 min. The austenitization at 900 °C is typical in case hardening applied in industry, and as such was selected as a reference in this study.

As expected, a microstructure composed of α' and some γ_{ret} is revealed for all selected conditions in the case steel, 0.76 wt.% C, and after austenitization at 900 °C for the core steel, as shown in Figure 2a,b, respectively. On the other hand, a mixed microstructure composed of α and $\alpha' + \gamma_{ret}$ in different proportions is obtained for the core steel after an austenitizing treatment at temperatures ranging from 850 °C to 830 °C, as shown in Figure 2c. The quantitative metallography results on the fraction of the different phases is shown in Table 3, where it is clear that ferrite fraction, V_α, decreases as T_γ and t_γ increases. In Table 3, it has been also included values of austenite carbon content as

determined applying the lever rule and neglecting the carbon content in α. As it can be seen, C_γ could be as high as 0.43 wt.% when the austenitization condition is such that α accounts for 32% of the microstructure, the relevance of these results will become clear in the following sections.

Table 3. For the 0.29 wt.% C alloy, metallographic measurements of proeutectoid ferrite (α) fraction V_α. V_γ stands for the amount of austenite at the mentioned T_γ-t_γ conditions. C_γ is the estimated carbon content in the austenite calculated as described in the main text. HV10 is at hardness Vickers load 10 kg.

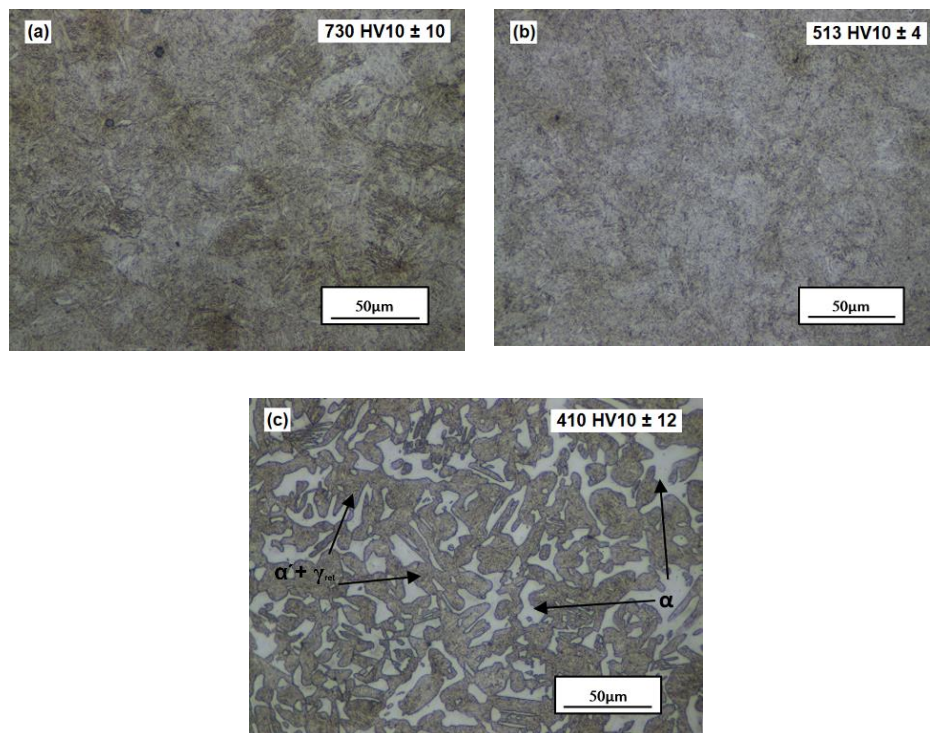| T_γ (°C)	t_γ (min)	V_α (vol %)	V_γ (= 1 − V_α) (vol %)	C_γ (wt.%)	HV10
900	30	0	100	0.29	513 ± 9
	15	0	100	0.29	525 ± 11
850	15	20 ± 3	80 ± 3	0.36	485 ± 10
	30	14 ± 2	86 ± 2	0.33	490 ± 8
840	15	25 ± 2	75 ± 1	0.38	450 ± 9
	30	20 ± 3	80 ± 2	0.36	466 ± 6
830	15	32 ± 2	68 ± 2	0.43	410 ± 12
	30	28 ± 3	72 ± 3	0.40	420 ± 10

Figure 2. Light optical micrographs of austenitized and quenched samples: (**a**) 0.76 wt.% C alloy after austenitized at 900 °C/30 min and for the 0.29 wt.% C (**b**) austenitized at 900 °C/30 min, (**c**) austenitized at 830 °C/15 min. Etched with Picral.

Note that that increasing the holding time from 15 to 30 min only determines a decrease on the α content of about 20–30%, while the structure of the matrix is quite similar. For this reason, the shorter holding time was selected for the following sections. Hardness results in Table 3 reflect the composite effect of the phases present on the microstructure, and thus the maximum value was obtained when a fully martensitic microstructure was present, decreasing this value progressively as the amount of α increases.

3.2. Characterization of Bainitic Transformation

Figure 3 shows the experimental Ms temperatures from Table 2, and those calculated using the Nehrenberg equation [19], based on the C_γ calculated in Table 3, and the chemistry of the bulk, Table 1. As it is shown, the predictions made by Nehrenberg are in close agreement with those experimentally obtained. It is clear that while for the case steel the Ms temperature is as low as 225 °C, for the core steel this temperature will range from 300 to 330 °C, after an austenitizing treatment at temperatures from 850 to 830 °C, since the presence of α will produce an increase of the austenite carbon content.
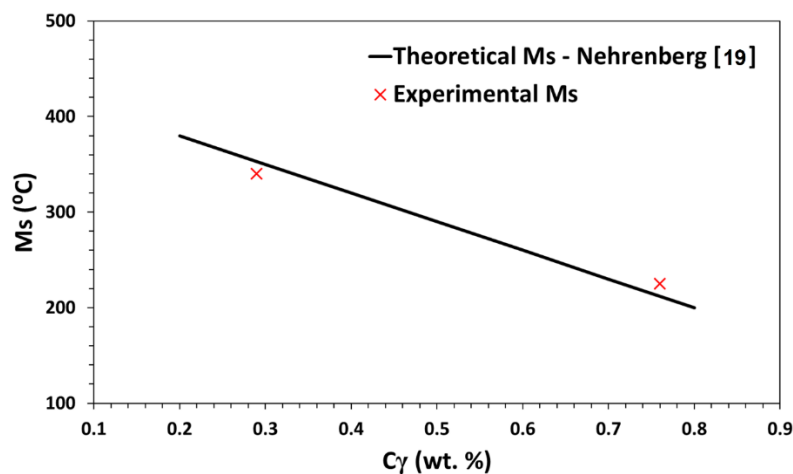

Figure 3. Theoretical Nehrenberg [19] and experimental Ms temperature as a function of carbon content in austenite, C_γ.

The isothermal heat treatment aims to obtain a nanobainitic structure in the case steel, thus T_{iso} of 250 and 300 °C were selected, which are close to the Ms of the case steel. In addition, to produce a multiphase microstructure of α, α_b and some α' or $\alpha' + \gamma_{ret}$ constituent in the core, the selected austenitizing condition was 830 °C/15 min. Finally, for comparison purposes, an austenitization at 900 °C/15 min was chosen to produce full austenitizing at the case and the core. The exact conditions for the treatments are given in Table 4. According to Bhadeshia [2], bainitic transformation becomes slower as austenite C content increases. Consequently, in order to ensure completion of the bainitic transformation, selected times for the isothermal treatment in Table 4 were made on the basis of researches reported by Garcia-Mateo et al. [20,21] of nanobainitic steels with similar chemistry to the case steel; therefore, t_{iso} of 480 and 240 min were selected for the 250 and 300 °C treatments, respectively.

Table 4. Heat treatment conditions for isothermal test. Where T_γ and T_{iso} stands for the austenitization and austempering temperature, respectively, whereas t_γ and t_{iso} stand for the respective times. CR_{iso} is the cooling rate from the austenitizing temperature to the temperature of the isothermal treatment.

C (wt.%)	T_γ (°C)	t_γ (min)	CR_{iso} (°C/s)	T_{iso} (°C)	t_{iso} (min)
0.29	900	15	35	250	480
				300	240
	830			250	480
				300	240
0.76	900			250	480
				300	240
	830			250	480
				300	240

Again, the selection of the cooling rate from T_γ down to T_{iso}, 35 °C/s, was done on the basis of both, avoid any transformation on cooling that might interfere with the whole process and using a cooling rate that can be reproduced at the industrial scale.

The dilatometric curves of the RCL vs. T and those corresponding to the isothermal part of the experiment (RCL vs. t) are shown in Figures 4 and 5 for the case and core steels, respectively. As can be observed in Figure 4, a reduction of the prior austenite grain size (PAGS), by lowering the austenitization temperature, reduces the activation of bainite transformation, and enhances the nucleation rate by the associated increase in the density of nucleation sites at grain boundaries, thus accelerating the bainite phase transformation (see, e.g., [22,23]). Regardless of the steel and test conditions, the remaining austenite is enriched by C during the bainitic transformation, increasing its stability to transform to martensite during cooling down to room temperature, as shown in Figures 4 and 5.
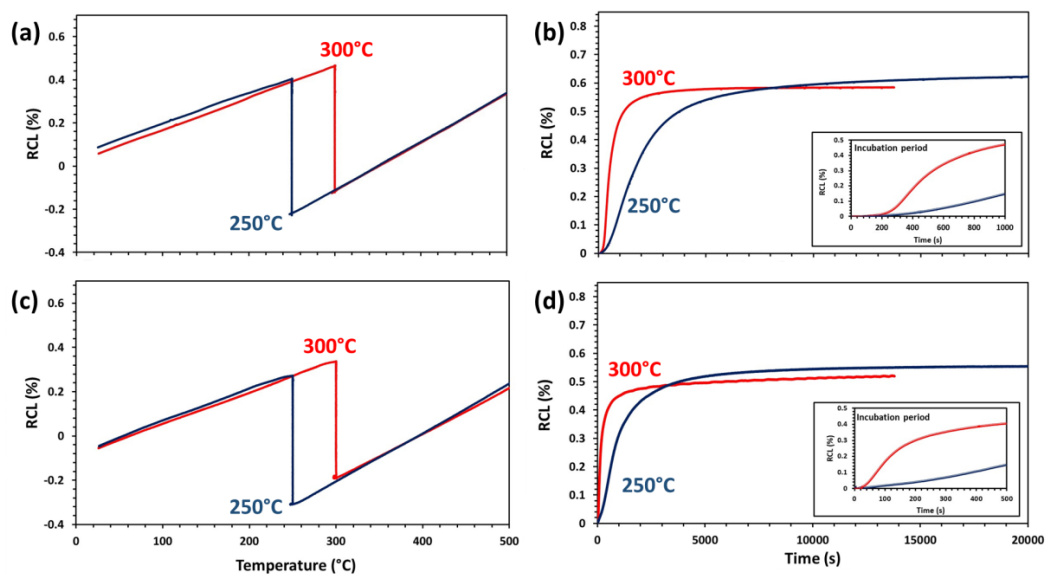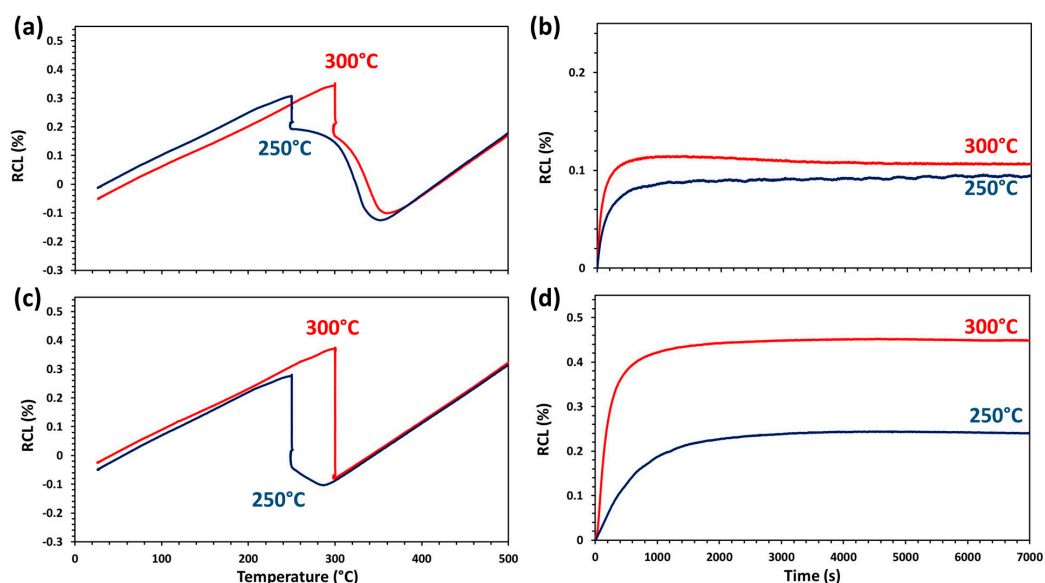

Figure 4. For the case steel (0.76 C wt.%), relative change in length (RCL) curves as a function of temperature and time for the different T_{iso}-t_{iso} (**a**) and (**b**) for T_γ = 900 °C and (**c**) and (**d**) T_γ = 830 °C.

Figure 5. For the core steel (0.29 Cwt.%), relative change in length (RCL) curves as a function of Temperature and time for the different T_{iso}-t_{iso} (**a**) and (**b**) for T_γ = 900 °C and (**c**) and (**d**) T_γ = 830 °C.

Table 5 collects microstructural characterization results based on XRD (V_γ and C_γ), systematic manual point count (V_α) and dilatometry ($V_{\alpha'}$), by applying the Koistinen–Marburger (K-M) expression as described by Navarro-Lopez et al. [24]. At this point, it must be clarified that martensite formed for the core alloy by quenching from 900 and 830 °C decomposes from body-centered tetragonal (BCT) martensite to body-centered cubic (BCC) ferrite and orthorhombic cementite during isothermal annealing at 300 and 250 °C. Additionally, it has to be recalled that the sample quenched from 830 °C and isothermally treated at 300 °C did not form martensite. As can be seen, the Ms values for the core steel in Tables 2 and 5 slightly differ, which is attributed to differences in the austenitizing temperatures (different PAGS) and differences in the quenching rates used for the dilatometric analysis, possible chemical microsegregations that are common in cast steels may have an influence as well. Bainitic ferrite fraction measurements correspond to $V_{\alpha b} = 100 - (V_\gamma + V_\alpha + V_{\alpha'})$ and its thickness, as well as that of the thin films of retained austenite, were measured according to the methodology described in the previous section. Examples of the obtained microstructures are shown for both steels in Figures 6 and 7. It is important to highlight that the presence of sufficient Si in the chemical composition of both steels can have impeded the formation of cementite during bainitic transformation, as reported by Arijit [25].

Table 5. Microstructural characterization data from the samples isothermally transformed. Where, V_γ and C_γ stand for the volume fraction and carbon content of austenite measured by XRD. V_α is the fraction of proeutectoid ferrite measured by point counting. From dilatometric curves the martensite start temperature, Ms and fraction of martensite $V_{\alpha'}$ are derived. Fraction of bainitic ferrite $V_{\alpha b} = 100 - (V_\gamma + V_\alpha + V_{\alpha'})$. Finally, $t_{\alpha b}$ and $t_{\gamma t}$ stands for the bainitic ferrite and retained austenite thin film thicknesses, respectively.

Alloy C (wt.%)	0.29				0.76			
	Isothermally treated samples							
T_γ(°C)/t_γ(min)	900/15		830/15		900/15		830/15	
T_{iso}(°C)/t_{iso}(min)	250/480	300/240	250/480	300/240	250/480	300/240	250/480	300/240
$t_{\alpha b}$ (nm)	168 ± 13	250 ± 13	135 ± 15	170 ± 16	58 ± 6	96 ± 18	54 ± 6	102 ± 18
$t_{\gamma t}$ (nm)	146 ± 14	195 ± 15	90 ± 14	140 ± 10	44 ± 6	70 ± 10	45 ± 9	65 ± 11
$V\alpha_b$ (Vol %)	25.5	34.5	25.3	58.5	85.5	83.3	86.7	85.1
$V\alpha'$ (Vol %)	70	56	36	-	-	-	-	-
$V\alpha$ (Vol %)	-	-	32.3 ± 3	33 ± 3	-	-	-	-
$V\gamma$ (Vol %)	4.5 ± 3	9.5 ± 3	6.7 ± 3	8.5 ± 3	14.5 ± 3	16.7 ± 3	13.3 ± 3	14.9 ± 3
$C\gamma$ (wt.%)	1.54 ± 0.12	1.67 ± 0.12	1.63 ± 0.12	0.79 ± 0.12	1.03 ± 0.12	1.24 ± 0.12	1.20 ± 0.12	1.33 ± 0.12
HV10	490 ± 9	440 ± 7	380 ± 6	340 ± 8	579 ± 4	513 ± 5	576 ± 6	510 ± 10
Ms (°C)	356	374	291	-	-	-	-	-

As expected, the case steel revealed the typical nanostructured bainite microstructure, as shown in Figure 6. In this microstructure, bainitic ferrite is the matrix, and presents a plate structure with thickness of about 54 and 102 nm for samples held at 250 and 300 °C, respectively—thicker plates at higher transformation temperatures. The carbon-enriched γ is the second dispersed phase, which shows two different morphologies, see Figure 6, as thin films between the α_b plates and as blocks separating the bainitic sheaves (groups of α_b plates that share a similar orientation), which, as expected, is thinner as more bainite forms, i.e., at lower transformation temperatures, see Table 5.

An example of the core steel multiphase structure is shown in Figure 7a,b, where a mixture of α + α_b + γ_{ret} + tempered α' in variable proportions depending on the T_γ and T_{iso} temperatures is revealed, see Table 5. The proeutectoid ferrite fraction, α, is determined by the intercritical austenitising condition and it should be the same for a given T_γ and both T_{iso} conditions. As anticipated by the dilatometric curves, the amount of tempered α' is much higher in the $T_\gamma = 900$ °C (Figure 7c,d) than that in the $T_\gamma = 830$ °C condition, see Table 5. It is worth noting that the scale of the bainitic microstructure obtained

in the core steel is far coarser than that of the case steel, with α_b plates and thin films thicknesses in the range of the submicrometric size, see Table 5 and Figure 7.
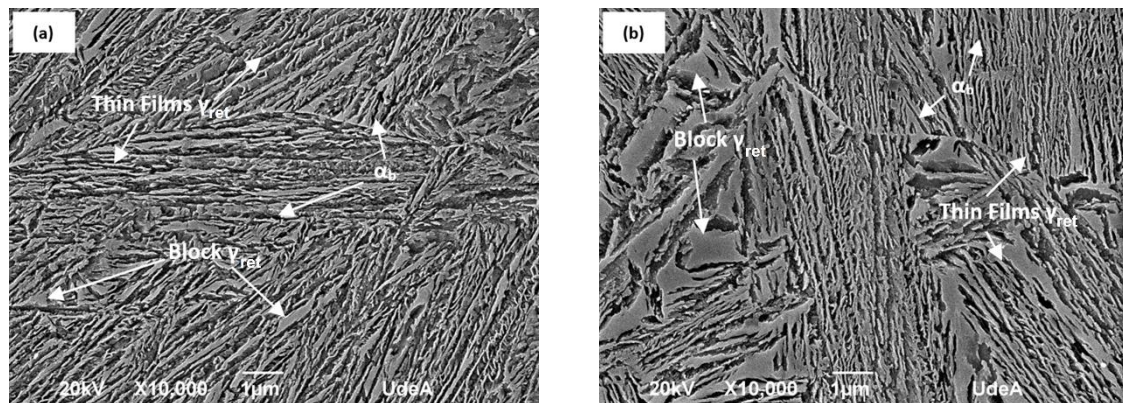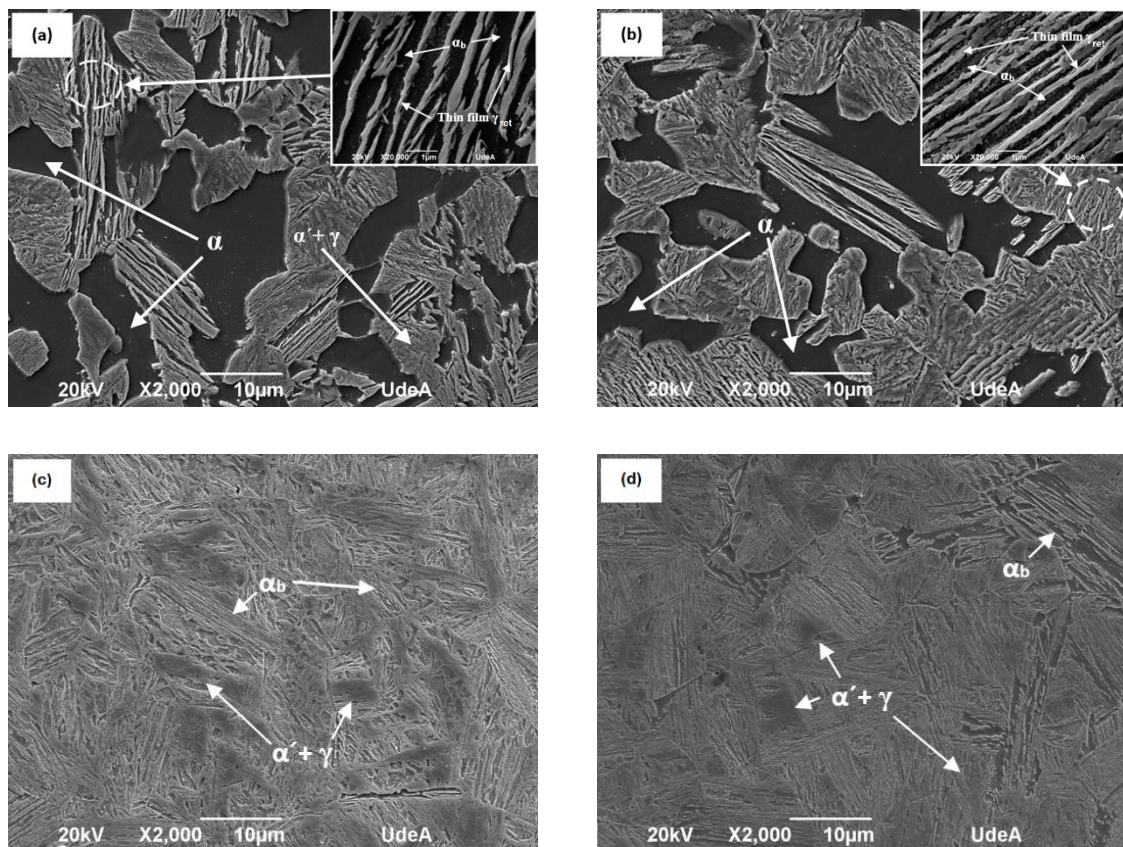

Figure 6. Secondary electron SEM images of the microstructure of the alloy with 0.76% of C, after austenitization at 830 °C/15 min., and treated isothermally at (**a**) 250 °C/480 min., and (**b**) 300 °C/240 min. Where γ_{ret} is austenite and α_b bainitic ferrite.

Figure 7. Secondary electron SEM images of the microstructure of the alloy with 0.29% of C, after austenitization at 830 °C, and treated isothermally at (**a**) 250 °C/480 min., and (**b**) 300 °C/240 min. and austenitization at 900 °C, and treated isothermally at (**c**) 250 °C/480 min., and (**d**) 300 °C/240 min. Where α is ferrite, $\alpha' + \gamma$ is martensite + austenite and α_b is bainitic ferrite.

In order to compare the results of the new heat treatments with those obtained after applying the material to the conventional industrial Q&T treatment, both steels were quenched from 900 °C and

then tempered at 250 °C for 120 min. The microstructures thus obtained are presented in Figure 8, consisting of tempered α' and some γ_{ret}.
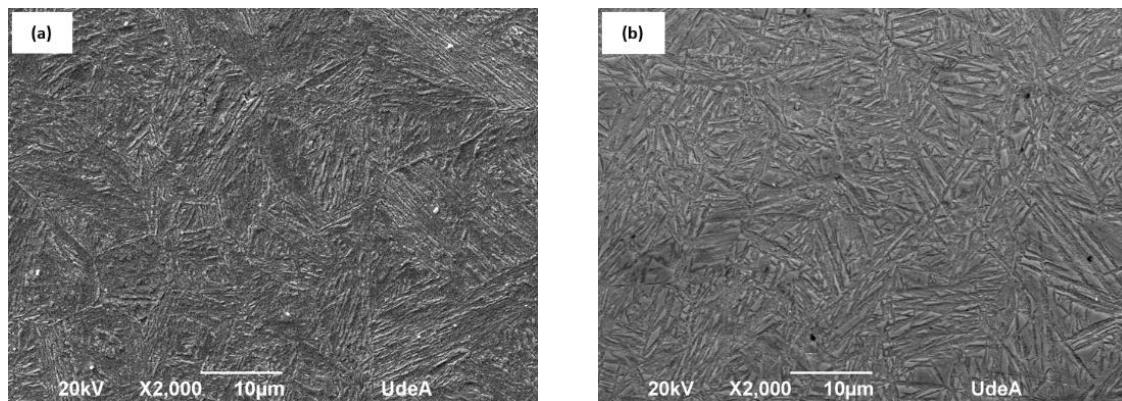

Figure 8. Secondary electron SEM images of the microstructure of the Q&T condition: (**a**) for core and (**b**) case steel.

3.3. Mechanical Properties

As already mentioned in a previous section, sub-size tensile and Charpy V-notched specimens where machined from the case steels prior to its carburization. The carbon profile of the carburized steel is shown in Figure 9, revealing that the surface C content is that of the case steel, ~0.76 wt.%, and the total case depth is about 1.6mm, which is comparable with that needed, as reported by Kramer [26], for commercial applications (e.g., pinions, gear wheels and power shafts).
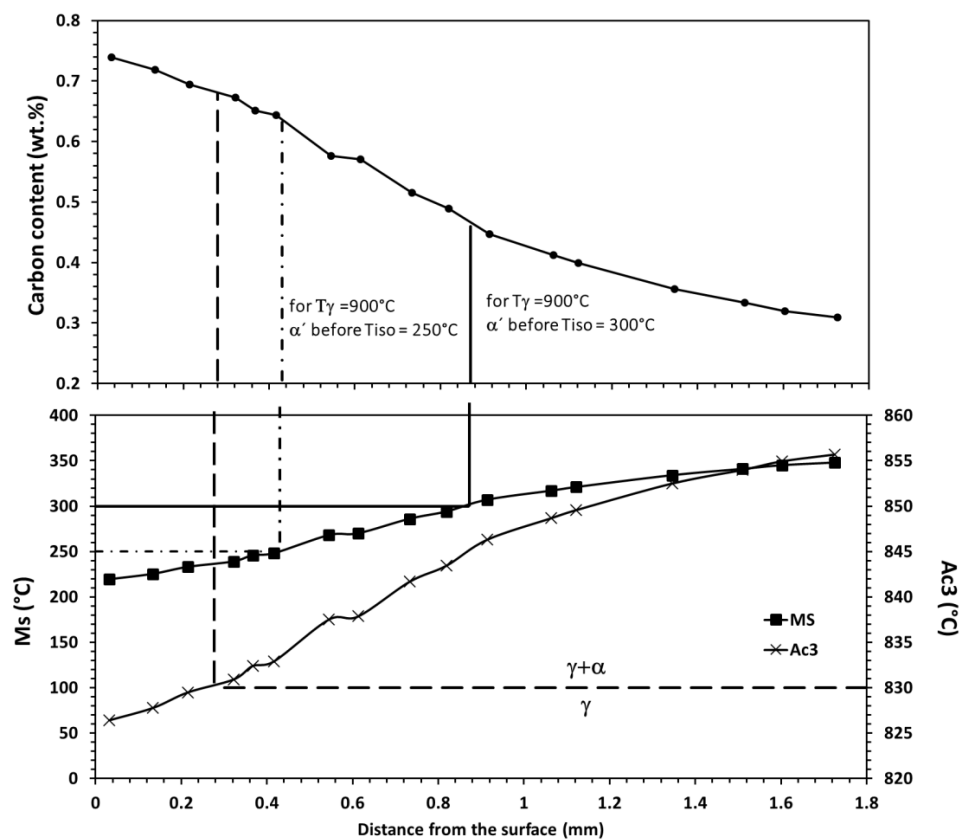

Figure 9. Carbon content distribution with depth from the carburized surface. Estimated Ms and Ac3 temperature as described in the main text.

In the same Figure 9, the estimated Ae3 and Ms for the corresponding C contents are also given. For the calculation of Ac3, the experimental values reported in Table 2 are taken assuming a linear dependence of this temperature with the C content and the Ms calculations are made based on Nehrenberg [19]. With these calculations in mind, the microhardness (HV 0.3) profiles obtained for each condition can be discussed, see Figures 10 and 11. Finally, in the Q&T condition, Figure 10, through the whole section, the microstructure is expected to be tempered martensite and austenite, where the C content of the α' and its tempering resistance are controlling the HV, i.e., continuous decrease from the case to the core.
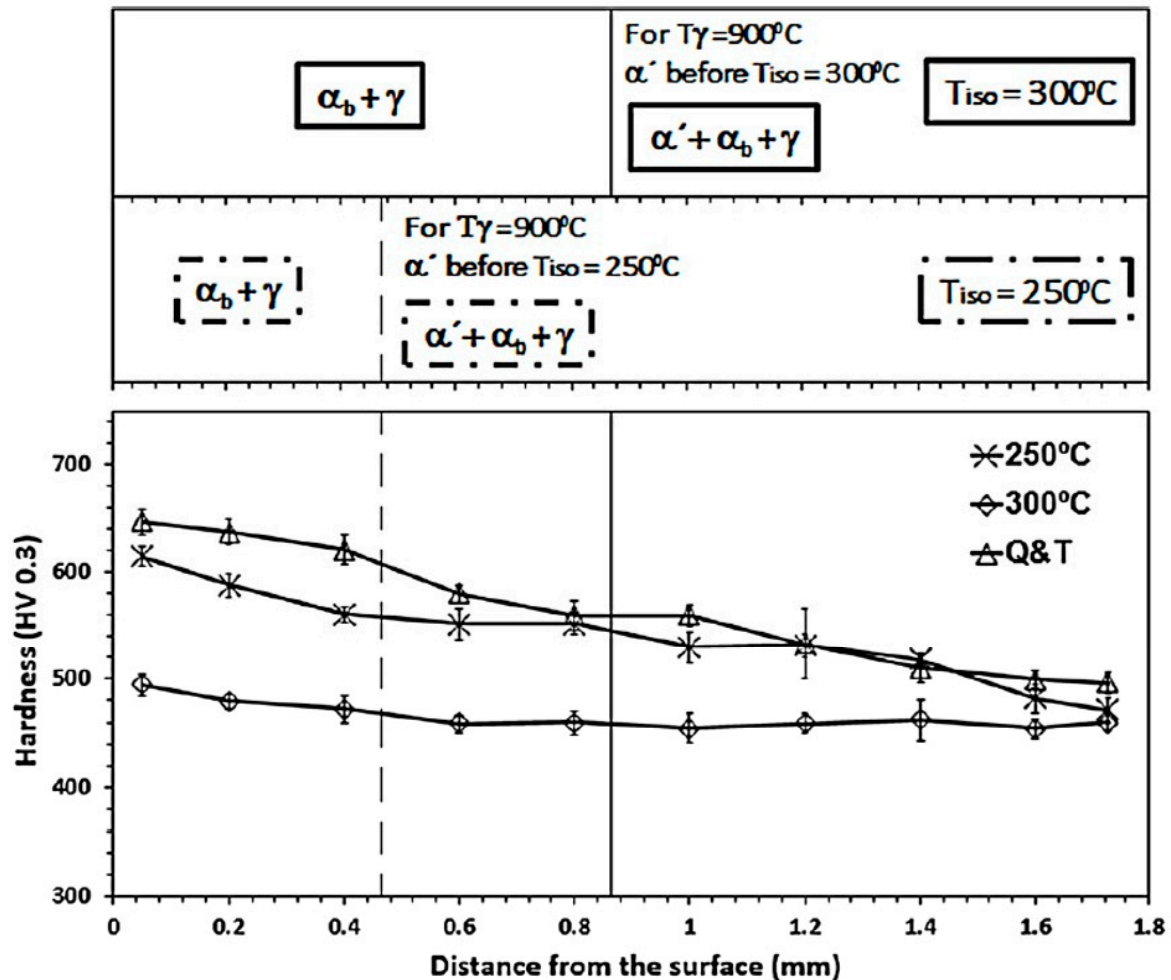

Figure 10. For T_γ = 900 °C. Hardness profiles of surface-carburized steels after conventional heat treatment (Q&T) and after isothermal heat treatments.

Figure 12 shows the stress–strain curves obtained for all conditions evaluated, and results extracted from the curves are gathered and summarized in Table 6. The specimens are characterized by continuous yielding, what is commonly attributed to mobile dislocations introduced during isothermal transformation, in accordance with reports by Garcia-Mateo et al. [27]. Discontinuous yielding is suppressed by the presence of many dislocation sources coming into action when at low strain the plastic flow begins simultaneously throughout the specimen. Plastic deformation is at first focused on the softer phase; the harder phase only begins to deform when the former has sufficiently strain hardened to transfer load, leading to a continuous yielding. As is evident in Figure 12, plastic deformation is uniformly distributed along the gauge length of the samples, showing little or no necking, meaning that most or all of the elongation is uniform.
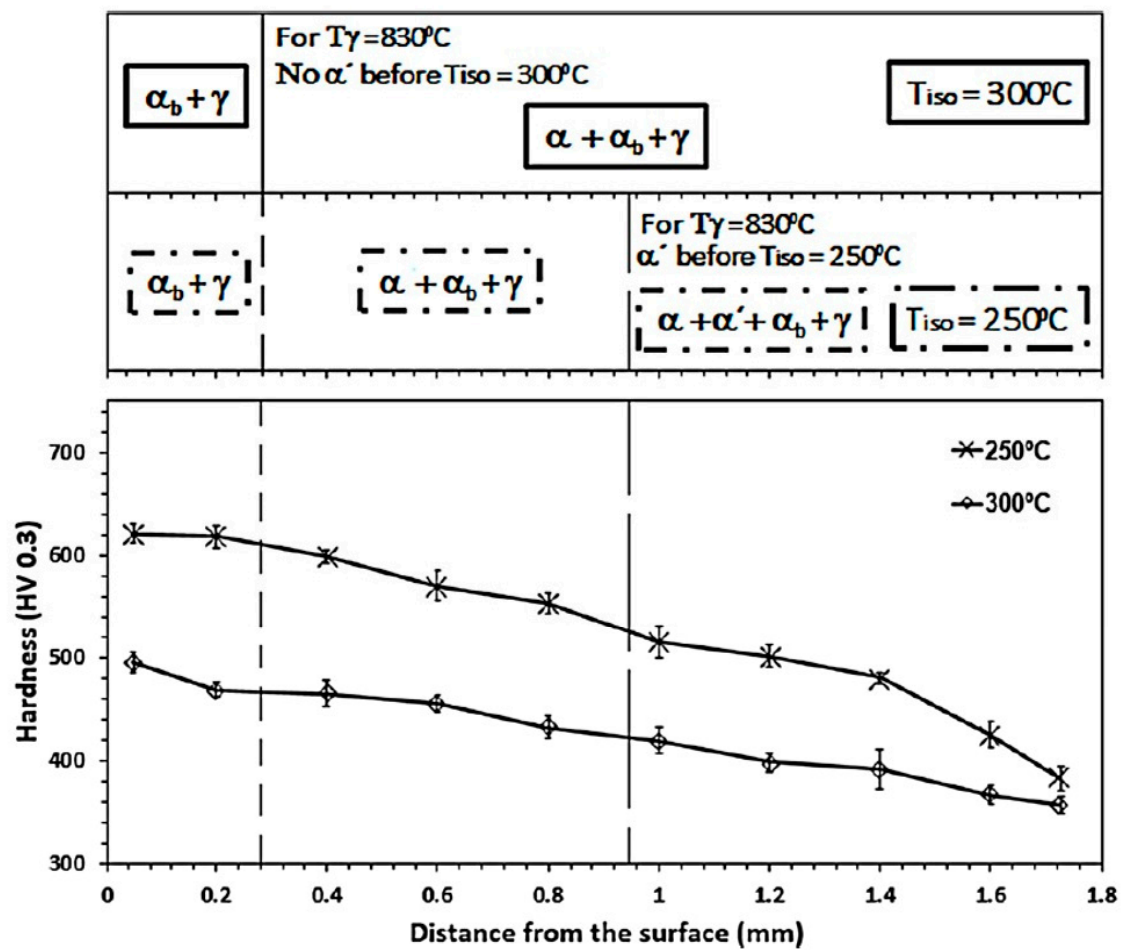
Figure 11. For T$_\gamma$ = 830 °C. Hardness profiles of surface-carburized steels after isothermal heat treatments.
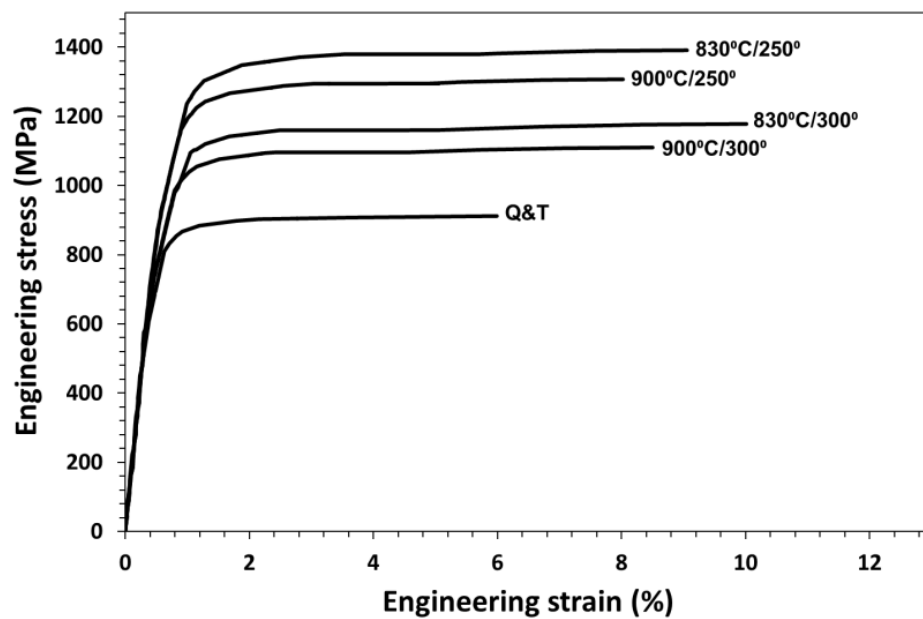

Figure 12. Engineering stress–strain curves at room temperature, of microstructures obtained after transformation at the temperatures indicated.

Table 6. Mechanical properties in carburized steel under different processes. Q&T: quenching and tempering; YS: yield strength; UTS: ultimate tensile strength; TE: total elongation; V-notch: impact energy.

T_γ/t_γ (°C/min)	T_{iso}/t_{iso} (°C/min)	YS (MPa)	UTS (MPa)	TE (%)	V-Notch (J)
900/15	Q&T	846 ± 13	911 ± 15	6.0 ± 0.5	4 ± 0.5
900/15	250/480	1220 ± 7	1310 ± 16	8.0 ± 0.4	6 ± 0.4
	300/240	1025 ± 26	1110 ± 17	8.5 ± 0.4	8 ± 0.8
830/15	250/480	1289 ± 5	1390 ± 26	9.0 ± 0.2	9 ± 0.3
	300/480	1106 ± 11	1179 ± 25	10 ± 0.2	12 ± 0.4

4. Discussion

4.1. Bainitic Transformation

As expected, for the case steel, the RLC-T curves show constant slope down to the isothermal bainitic transformation temperature, indicating that no phase transformation occurred during cooling. However, for the core steel, this behavior depends on the applied T_γ. Thus, while for full austenitization, T_γ = 900 °C, martensitic transformation is observed around 360–370 °C, with a higher degree of transformation for the T_{iso} = 250 °C, for T_γ = 830 °C martensite (α') only forms when cooling to 250 °C, at 291 °C. Those results are in line with the expected C enrichment of austenite when austenitizing in the $\alpha + \gamma$ field, i.e., intercritical austenitization at 830 °C. Note that the observed Ms temperature, Table 5, fits well with that estimated in Figure 3, corroborating the validity of the performed calculations.

The sigmoidal curve obtained during isothermal bainitic transformation, Figures 4b–d and 5b–d, has a first stage named incubation time during which the transformation has not yet started, or it is not yet detectable by the experimental techniques used. The core steel shows almost no incubation time. On the other hand, for the case steel, bainitic transformation starts after an incubation time of 400 and 200 s at 250 and 300 °C, respectively, and for T_γ = 830 °C these incubation times are even shorter, an effect that can be attributed to the accelerating effect on bainitic transformation when decreasing the prior austenite grain size (PAGS) [22,23]. It is also worth noting that, in any case, the reported incubation times are much shorter than those reported by Garcia-Mateo et al. [28] for wrought steels of similar chemical composition, 1.0 and 0.8 C (wt.%). The short incubation times for the case steel can be associated with the formation of acicular bainite in non-metallic inclusions and a concomitant catalytic effect on the bainitic reaction, local chemistry variations associated with chemical microsegregation in the cast steel may have an influence as well. However, currently there are not enough data and this matter can be the subject of future research.

A second stage in the curve, where nucleation and growth occur, is characterized by a steady and continuous increase of the RCL, leading to the final stage where no further transformation occurs and a steady state or plateau is reached. The times to reach the end of the transformation, contained within the plateau of the RCL curve, were calculated according to the procedures described by Santajuana et al. [29] with a threshold of zero. The results thus obtained for the 0.76 wt.% C showed that, regardless of the chosen T_γ, at 250 °C, 4 h are needed while at 300 °C the transformation only needed 2 h. In the case of the core steel, the times are drastically reduced to 20 and 12 min, for T_γ = 900 °C, and to 40 and 25 min, for T_γ = 830 °C, for the transformation at 250 and 300 °C, respectively. The results also agree with the bainite transformation theory reported by Bhadeshia [2] in terms of slower transformation, as the transformation temperature decreases and/or C of the transforming austenite increases.

According to the To line theory, development by Bhadeshia [2], that rules the bainitic transformation, it is expected that the lower the transformation T and/or the C content of the parent γ, the higher is the amount of α_b that it forms, and that should be directly linked to higher RCL-t dilatometric curves. It is clear that, this being the case for the 0.76 wt.% C steel, Figure 4b,d, it is not for the core steel.

Figure 5b,d show that a large amount of austenite transforms to martensite before isothermal holding, and under this condition much less ferritic bainitic may be transformed from residual austenite and the principal microestructural change is the tempering of the martensite.

4.2. Mechanical Properties

The tensile and Charpy V-notched impact energy tests were conducted at room temperature in samples heat-treated under the conditions just described, and results thus obtained are summarized in Table 6. Given that the phase composition and microstructure change gradually from the surface to the core (see Figures 10 and 11) in the tensile and Charpy specimens, the description of the mechanisms behind the mechanical behavior are very complicated, and, therefore, it is hard to reach clear conclusions. The next paragraphs intend to throw some light on these matters.

The results showed that, regardless of the austenitization T, in terms of strength (YS and UTS), ductility (TE) and impact energy, the microstructures obtained by isothermal heat treatment performed much better than those obtained by the more traditional Q&T treatment. Regarding the effect of the isothermal heat treatment temperature, at 250 °C the microstructures are stronger but toughness and ductility suffer and are lower than in the case of treatment at 300 °C, which is rationalized in terms of a higher fraction of martensite through the section of the sample. As for the effect of T_γ, data of microstructural characterization in Table 5 show, for a given value of the T_{iso}, that although austenitization at 830 °C instead at 900 °C will only produce small variations in the microstructural parameters and hardness value of the case steel, it will have a rather marked effect in the core of carbo-austempered samples at both isothermal quenching temperatures. Table 5 shows that intercritical austenitization at 830 °C gives to the core the same or higher fraction of bainitic ferrite and thinner bainitic ferrite and austenite films, which improves strength when compared with samples austenitized at 900 °C, together with a high amount of unstransformed ferrite, which being more effective than martensite and bainitic ferrite to accommodate plastic strain will improve ductility and impact toughness of carburized steel, as shown in Table 6.

For the T_γ = 900 °C condition, Figure 10, from the surface to the core, the material is fully austenitized previous to the isothermal treatment. Based on the calculation shown in Figures 9 and 10 indicates with vertical lines the depth at which martensitic transformation is expected to occur depending on the isothermal T. Note that those calculation agrees with previous experimental observations in Figures 4 and 5. It is evident that in the region where only α_b and γ_{ret} is expected in the microstructure, as the C content decreases, and more α_b forms, HV gently decreases for both T_{iso}, the reduction is associated with thicker α_b plates. Differences in the HV values between both transformations T are also justified in the same terms, i.e., more α_b and thinner at T_{iso} = 250 °C than at T_{iso} = 300 °C.

Once α' appears in the microstructure, previous to the isothermal treatment, it has been already discussed that there is less bainitic transformation. Thus, as the core is approached, the microstructure is composed of tempered $\alpha' + \alpha_b + \gamma_{ret}$ with increasing quantities of tempered α' in detriment of that of α_b and γ_{ret}. While the drop in HV for the 250 °C treatment is only 50 units, in the 300 °C case HV is almost negligible as less α' is forming as compared to lower temperature treatment. Close to the core, the reported HV values are in line with those presented in Table 5, which is an indicative that the selected heat treatments were successfully applied.

For the discussion of the HV profile with T_γ = 830 °C, the situation is a bit more complex, as we have to consider that, while there are regions of the material that are fully austenitized—see vertical lines in Figure 9—there are other regions that are in the $\alpha + \gamma$ field, and the austenite is then C enriched (γ^+). Such enrichment, as it has been shown, implies that Ms temperatures are lower than those calculated for the T_γ = 900 °C. For the core steel, it was estimated that the C content of the of austenite ($\gamma+$) at T_γ = 830 °C was 0.43 wt.%, see Table 3, and the calculated Ms temperature for that C level in Figure 9 (~300 °C) is similar to that experimentally determined, see Table 5. Using this same approach, if we consider now that, at a depth of 0.95 mm, a C content of 0.44 wt.% was measured,

see Figure 9; thus, when that part of the carburized steel is heated at T_γ=830 °C it is in the $\alpha + \gamma$ field, see Figure 9, and it is estimated that the austenite contains about 0.64 wt.% C. In this same Figure 9, the Ms temperature for a 0.64 wt.% C is ~250 °C, meaning that if T_{iso} is 300 °C, martensite should not be expected in the whole depth, while if Tiso is decreases to 250 °C, martensite will appear from a depth of 0.95 mm to the core. By using this same type of calculations and attending to the results in Figure 9, it is possible to prepare Figures 10 and 11 to gather all these results in a schematic way.

As in the case of full austenitization, when only $\alpha_b + \gamma_{ret}$ is expected in the microstructure, as the C content decreases, and more α_b forms, HV gently decreases for both T_{iso}, the reduction is associated with thicker α_b plates, and the small differences found with the case of $T_\gamma = 900$ °C, again indicates the little effect that PAGS might have for those chemical compositions on the resulting α_b. The presence of proeutectoid ferrite into mixed microstructures of $\alpha + \alpha_b + \gamma_{ret}$, leads to a gentle decrease of the HV, as more α in detriment of α_b is present in the microstructure—see, for example, the case of the $T_{iso} = 300$ °C. The formation of α', $T_{iso} = 250$ °C, reduced the amount of α_b, and it results in a more step decrease in HV values. As before, close to the core, the reported HV values are in line with those presented in Table 5.

5. Conclusions

Carbo-austempered steels with nanobainitic microstructures (α_b and γ) in the case and multiphasic microstructures ($\alpha + \alpha_b +$ tempered $\alpha' + \gamma$) in the core can be achieved by properly selecting the austenitizing temperature followed by isothermal transformation at the bainitic temperature range.

Tensile properties and impact toughness of carbo-austempered steels are related with the complex nature of their microstructures, which include through the thickness of the sample different amounts of structural components with antagonistic properties like ferrite, bainite, martensite and austenite. For these materials, better mechanical properties than those achieved by a conventional Q&T process can be obtained by properly selecting the austenitizing temperature followed by isothermal transformation at the bainitic temperature range, to reach nanobainitic microstructures (α_b and γ) in the case and multiphasic microstructures ($\alpha + \alpha_b +$ tempered $\alpha' + \gamma$) in the core. Tensile properties and impact toughness were favored by intercritically austenitizing, which gives a multiphasic microstructure in the core with a high amount of untransformed ferrite that is more effective to accommodate plastic strain than martensite and bainitic ferrite. The analysis of the wear and fatigue behavior is necessary to fully assess the performance of the developed nanobainitic carbo-austempered cast steels, which can be the topics for future investigations.

References

1. Bhadeshia, H.K.D.H.; Edmonds, D.V. The mechanism of bainite formation in steels. *Acta Metall.* **1980**, *28*, 1265–1273. [CrossRef]
2. Bhadeshia, H.K.D.H. *Bainite in Steels. Transformations, Microstructure and Properties*, 3rd ed.; Bhadeshia, H.K.D.H., Ed.; Institute of Materials, Minerals and Mining: London, UK, 2015.
3. Garcia-Mateo, C.; Caballero, F.G. Understanding the mechanical properties of nanostructured bainite. In *Handbook of Mechanical Nanostructuring*; Aliofkhazraei, M., Ed.; Wiley: Weinheim, Germany, 2015; Volume 1, pp. 35–65.

4. Caballero, F.G.; Morales-Rivas, L.; Garcia-Mateo, C. Retained austenite: Stability in a nanostructured bainitic steel. In *Encyclopedia of Iron, Steel, and Their Alloys*; Taylor & Francis: Abingdon, UK, 2016; pp. 3077–3087.

5. Hayrynen, K.; Brandenberg, K.; Keough, J.R. *Carbo-Austempering™—A New Wrinkle?* SAE Technical Paper; SAE: Warrendale, PA, USA, 2002. [CrossRef]

6. Damon, J.; Mühl, F.; Dietrich, S.; Schulze, V. A Comparative Study of kinetic models regarding bainitic transformation behavior in carburized case hardening steel 20MnCr5. *Metall. Mater. Trans. A* **2018**, *50*, 104–117. [CrossRef]

7. Zhang, F.C.; Wang, T.S.; Zhang, P.; Zheng, C.L.; Lv, B.; Zhang, M.; Zheng, Y.Z. A novel method for the development of a low-temperature bainitic microstructure in the surface layer of low-carbon steel. *Scr. Mater.* **2008**, *59*, 294–296. [CrossRef]

8. Zhang, F.; Yang, Z. Development of and perspective on high-performance nanostructured bainitic bearing steel. *Engineering* **2019**, *5*, 319–328. [CrossRef]

9. Morales-Rivas, L.; Garcia-Mateo, C.; Sourmail, T.; Kuntz, M.; Rementeria, R.; Caballero, F. Ductility of nanostructured bainite. *Metals* **2016**, *6*, 302. [CrossRef]

10. International, A.S.T.M. *Standard Test Methods for Determining Average Grain Size*; ASTM E112-13; ASTM International: West Conshohocken, PA, USA, 2013.

11. International, A.S.T.M. *Standard Test Method for Determining Volume Fraction by Systematic Manual Point Count*; ASTM E562-19; ASTM International: West Conshohocken, PA, USA, 2019.

12. Garcia-Mateo, C.; Jimenez, J.A.; Lopez-Ezquerra, B.; Rementeria, R.; Morales-Rivas, L.; Kuntz, M.; Caballero, F.G. Analyzing the scale of the bainitic ferrite plates by XRD, SEM and TEM. *Mater. Charact.* **2016**, *122*, 83–89. [CrossRef]

13. Dyson, D.J.; Holmes, B. Effect of alloying additions on lattice parameter of austenite. *J. Iron Steel Inst.* **1970**, *208*, 469–474.

14. International, A.S.T.M. *Standard Test Methods for Tension Testing of Metallic Materials*; ASTM E8/8M-16a; ASTM International: West Conshohocken, PA, USA, 2016.

15. International, A.S.T.M. *Standard Test Methods for Notched Bar Impact Testing of Metallic Materials*; ASTM E23-16b; ASTM International: West Conshohocken, PA, USA, 2016.

16. Parrish, G. *Carburizing: Microstructures and Properties*; ASM International: Novelty, OH, USA, 1999; p. 222.

17. de Andres, C.G.; Caballero, F.G.; Capdevila, C.; Alvarez, L.F. Application of dilatometric analysis to the study of solid-solid phase transformations in steels. *Mater. Charact.* **2002**, *48*, 101–111. [CrossRef]

18. Sourmail, T.; Smanio, V. Determination of Ms temperature: Methods, meaning and influence of 'slow start' phenomenon. *Mater. Sci. Technol.* **2013**, *29*, 883–888. [CrossRef]

19. Nehrenberg, A.E. The temperature range of martensite formation. *Trans. ASM* **1946**, *167*, 494–498.

20. Garcia-Mateo, C.; Caballero, F.; Bhadeshia, H.K.D.H. Development of hard bainite. *ISIJ Int.* **2003**, *43*, 1238–1243. [CrossRef]

21. Caballero, F.G.; Garcia-Mateo, C.; Sourmail, T. Bainitic Steel: Nanostructured. In *Encyclopedia of Iron, Steel, and Their Alloys*; Taylor & Francis: Abingdon, UK, 2016; pp. 271–290.

22. Garcia-Mateo, C.; Caballero, F.G.; Bhadeshia, H.K.D.H. Acceleration of Low-temperature Bainite. *ISIJ Int.* **2003**, *43*, 1821–1825. [CrossRef]

23. Li, Z.; Li, P.; Luo, Y.; Zhou, X.; Qi, L.; Li, S.; Wang, Z. Effect of austenitizing temperature and prior martensite on ultra-fine bainite transformation kinetics. *Metals* **2019**, *9*, 1309. [CrossRef]

24. Navarro-López, A.; Sietsma, J.; Santofimia, M.J. Effect of prior athermal martensite on the isothermal transformation kinetics below Ms in a low-C high-Si steel. *Metall. Mater. Trans. A* **2016**, *47*, 1028–1039. [CrossRef]

25. Saha Podder, A. Tempering of a Mixture of Bainite and Retained Austenite. Ph.D. Thesis, University of Cambridge, Cambridge, UK, 2011.

26. Kramer, P.C. An Investigation of Rolling-Sliding Contact Fatigue Damage of Carburized Gear Steels. Ph.D. Thesis, Colorado School of Mines, Golden, CO, USA, 2014.

27. Garcia-Mateo, C.; Caballero, F.G. Ultra-high-strength bainitic steels. *ISIJ Int.* **2005**, *45*, 1736–1740. [CrossRef]

28. Garcia-Mateo, C.; Caballero, F.G. Nanocrystalline bainitic steels for industrial applications. In *Nanotechnology for Energy Sustainability*; Wiley-VCH Verlag GmbH & Co. KGaA: Weinheim, Germany, 2017; pp. 707–724. [CrossRef]

29. Santajuana, M.A.; Eres-Castellanos, A.; Ruiz-Jimenez, V.; Allain, S.; Geandier, G.; Caballero, F.G.; Garcia-Mateo, C. Quantitative assessment of the time to end bainitic transformation. *Metals* **2019**, *9*, 925. [CrossRef]